A macrocyclic receptor containing two viologen species connected by conjugated terphenyl groups

Article

Accepted Version

Journal Name

ARTICLE

A macrocyclic receptor containing two viologen species connected by conjugated terphenyl groups

Long Chen,[a] Kate J. C. Lim,[a] Tahkur S. Babra,[a] James O. Taylor,[a] Martin Pižl,[b,c] Robert Evans,[d] Ann M. Chippindale,[a] František Hartl,[a] Howard M. Colquhoun*[a] and Barnaby W. Greenland*[a,e]

A macrocyclic receptor molecule containing two viologen species connected by conjugated terphenyl groups has been designed and synthesised. The single-crystal X-ray structure shows that the two viologen residues have a transannular N…N separation of ca. 7.4 Å. Thus, the internal cavity dimensions are suitable for the inclusion of π-electron-rich species. The macrocycle is redox active, and can accept electrons from suitable donor species including triethylamine, resulting in a dramatic colour change from pale yellow to dark green as a consequence of the formation of a paramagnetic bis(radical cationic) species. Cyclic voltammetry shows that the macrocycle can undergo two sequential and reversible reduction processes ($E_{1/2}$ = -0.65 and -0.97 V vs Fc/Fc^+). DFT and TD-DFT studies accurately replicate the structure of the tetracationic macrocycle and the electronic absorption spectra the three major redox states of the system. These calculations also showed that during electrochemical reduction, the unpaired electron density of the radical cations remains relatively localised within the heterocyclic rings. The ability of the macrocycle to form supramolecular complexes was confirmed by the formation of a pseudorotaxane with a guest molecule containing a π-electron-rich 1,5-dihydroxynaphthalene derivative. Threading and dethreading of the pseudorotaxane was fast on the NMR timescale, and the complex exhibited an association constant of 150 M^{-1} (± 30 M^{-1}) as calculated from ^1H NMR titration studies.

Introduction

The field of supramolecular chemistry has developed dramatically over the last 30 years. In particular, it has moved, from fundamental studies of the interactions between molecules to the design and synthesis of highly complex but fully-defined structures, including mechanically interlocked molecules and supramolecular materials.[1–3] The dynamic and reversible nature of supramolecular bonds has resulted in the realisation of functional materials and nano-scale machines, including those that can undergo controlled switching[4–6] or rotation.[7,8]

Within the extensive literature of supramolecular chemistry, the *N,N'*-disubstituted 4,4'-bipyridinium (viologen) residue has become one of the most important and well-studied building blocks. Viologen dications are π-electron-poor species that undergo two sequential one-electron reductions to form firstly a radical cation and secondly a neutral quinoidal species.[9] In the dicationic state, they are able to form π-stacked supramolecular assemblies with a range of π-electron-rich aromatic compounds, especially those containing 1,5-dihydroxynaphthalene or tetrathiafulvalene residues.[10,11] More recently, supramolecular systems have also been constructed that harness interactions between singly-reduced radical-cationic viologen units[12–14] to form a distinct class of responsive macrocycles,[15] polymers[16] and mechanically interlocked systems.[17–19] Moreover, viologens and their radical cations are also integral components in a range of electronically conductive materials.[20–28]

One of the most widely studied viologen-based macrocycles is cyclobis(paraquat-*p*-phenylene) (CBPQT) that was first investigated as a supramolecular host molecule by Stoddart and co-workers in 1988 (**1**, Figure 1A).[29] In common with many more recent viologen-containing cyclophanes[30–34] and related supramolecular structures based on stacking interactions,[35–40] the separation of the π-electron-deficient residues in CBPQT is approximately 7 Å,[41] which is ideal for the inclusion – at about van der Waals' contact distance – of planar π-electron-rich or radical cationic compounds.[42,43] However, a drawback of CBPQT in terms of chemical stability is that it contains four *N*-benzylbipyridinium moieties that are known to be susceptible to rapid cleavage under nucleophilic[44] or basic conditions.[45]

Our own work in this area has focused on the synthesis of viologen-containing macrocycles[46,47] (for example $\mathbf{2}^{2+}$, Figure 1B) and conjugated oligomers[48–50] that do not contain *N*-benzylbipyridinium linkages. Specifically, we have synthesised macrocycles that feature either one or two viologen residues suitably positioned to form π–π stacked complexes and contain aromatic rather than aliphatic residues bound to each pyridinium ion. These viologen species are accessed using the Zincke reaction[51] that involves condensation of nucleophilic amines with *N*-(2,4-dinitrophenyl)pyridinium salts. First reported in 1904, the Zincke reaction remains one of the most efficient ways to access *N*-substituted aromatic pyridinium residues.[52] The Zincke reaction has recently been used by our group,[46–49] and others[53,54] to produce conjugated, viologen-based oligomers and metal-organic frameworks.[55,56]

[a] *Department of Chemistry, University of Reading, Whiteknights, Reading, RG6 6AD, UK;* email: h.m.colquhoun@reading.ac.uk
[b] *J. Heyrovský Institute of Physical Chemistry, Academy of Sciences of the Czech Republic, Dolejškova 3, CZ-182 23 Prague, Czech Republic*
[c] *Department of Inorganic Chemistry, University of Chemistry and Technology, Prague, Technická 5, CZ-166 28 Prague, Czech Republic*
[d] *Aston University Institute of Materials Research, School of Engineering and Applied Science, Birmingham, B4 7ET, UK.*
[e] *Department of Chemistry, School of Life Sciences, University of Sussex, Falmer, BN1 9QJ, UK; email b.w.greenland@sussex.ac.uk*

Electronic Supplementary Information (ESI) available: NMR spectra for new compounds, DOSY spectra, X-ray structure data, further TD-DTF analysis. See DOI: 10.1039/x0xx00000x

In common with all viologen-containing systems, the macrocyles we have synthesised and studied are electron acceptors, undergoing addition of a single electron to form paramagnetic, radical cationic species on contact with electron donors, such as triethylamine. ^{1}H NMR studies showed that the unpaired electron density was delocalised over the viologen and the aromatic substituents directly attached to the bipyridinium nitrogens (Figure 1B, **2**$^{\bullet+}$). In this example, further delocalisation around the entire macrocyclic ring is presumably prevented by the break in conjugation at the ether linkage between two aromatic rings.

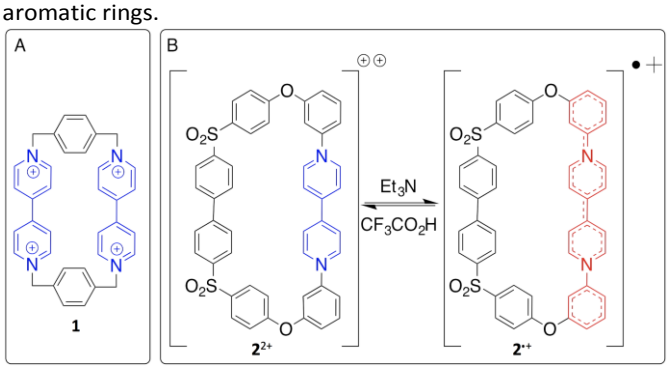

Fig. 1 (A) Structure of CBPQT (**1**) containing four chemo-labile *N*-benzylbipyridinium residues; (B) Scheme showing a viologen containing macrocycle ($\mathbf{2}^{2+}$) that does not contain *N*-benzylbipyridinium residues and its reversible reduction to a radical cation ($\mathbf{2}^{\bullet+}$). Aromatic and heterocyclic rings shown in red in $\mathbf{2}^{\bullet+}$indicate the region of delocalized, unpaired electron density.

Here, we report the design and synthesis of a novel bis-viologen cyclophane ($\mathbf{4}^{4+}$) that does not contain ether linkages or chemically labile *N*-benzylbipyridinium bonds. The new macrocycle contains 10 aromatic/heterocyclic rings that are not separated by either sp^3 carbon centres or ether bonds (as in **1** and **2**) yet can still form pseudorotaxanes with π-electron-rich species. In addition, it undergoes reversible chemical and electrochemical oxidation and reduction, making it ideally suited for the design of novel, responsive, interlocked systems.

Results and Discussion

Macrocycle and receptor design and synthesis

A key design criterion for the proposed macrocyclic receptor was the need to replace the benzylic unit in CBPQT (**1**, Figure 1) with a fully conjugated species whilst retaining a cavity size suitable for the inclusion of π-electron-rich species (*ca.* 7 Å). Computational modelling using molecular mechanics (Materials Studio v. 7.0) suggested that, in the *syn* conformation, the two nitrogen atoms in *m*-terphenylene diamine[57,58] (**3**, Scheme 1) would have a separation of ca. 7.3 Å, which should ultimately result in a macrocyclic species with appropriate internal dimensions for the formation of host/guest complexes with π-electron-rich aromatic species.

The synthesis of *m*-terphenylene diamine (**3**) was achieved in two steps (Scheme 1). Firstly, the double addition of 3-nitrophenyl boronic acid (**5**) to 1,3-dibromobenzene (**6**) was carried out under typical Suzuki conditions[59] to furnish **7** in 67% yield. Subsequently, the nitro groups on **7** were reduced to amino substituents in essentially quantitative yield using palladium catalysis, with poly(methylhydrosiloxane) (PMHS) as the hydrogen source.[60] The targeted macrocycle was then produced in a single step by the reaction of the di-Zincke salt **8** with diamine **3** under dilute conditions. Finally, ion exchange resulted in the isolation of $\mathbf{4}^{4+}$ (10% yield) which was soluble in polar organic solvents such as acetonitrile, acetone and DMF.

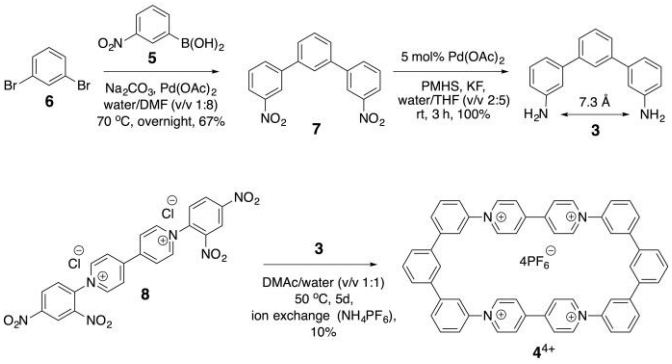

Scheme 1 Synthesis of macrocycle $\mathbf{4}^{4+}$.

It would be expected that π-electron-poor cyclophanes such as $\mathbf{4}^{4+}$ should form pseudorotaxane-type complexes with a range of π-electron-rich species. We selected the substituted naphthalene derivatives **9** and **10** as the first candidates for these studies because closely related structures have been found to bind to the cavity of a previous generation of viologen-type cyclophanes (for example, $\mathbf{2}^{2+}$, Figure 1).[46,47] The tri-naphthalene species **10** was readily accessed in 57% yield over two steps by tosylation of diol **9** to give **11** (ref.[61]), followed by Williamson ether synthesis to give the target compound **11** with three π-electron rich naphthalene residues. The oligoether groups in **9** and **10** have three distinct functions: i) to increase the solubility of the naphthalene residues; ii) to enable the naphthalene residues to adopt the ideal orientation for maximising π–π stacking interactions during complex formation; and iii) to enable the oxygen atoms in the ether linkages to form hydrogen bonds with the relatively acidic protons on the pyridinium rings, which are known to assist complex formation.[62]

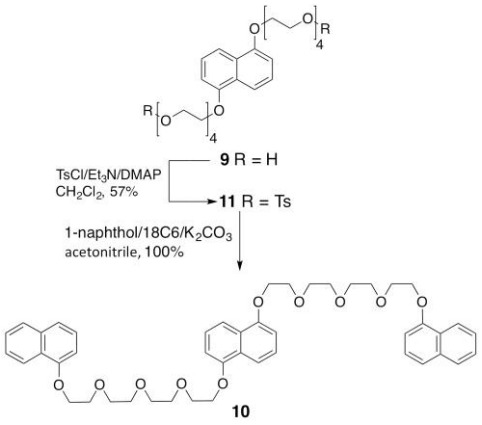

Scheme 2. Synthesis of the π-electron-rich tris(naphthalene) derivative **10** from diol **9**.

Macrocycle structure and electrochemical properties

Crystals of the macrocycle $\mathbf{4}^{4+}$ as its hexafluorophosphate salt suitable for X-ray structure determination were obtained by vapour diffusion of diethyl ether into an acetonitrile solution (Figure 2). The macrocycle adopts a relatively flattened conformation, with the 4,4'-bipyridinium rings rotated inwards toward the centre of the molecule, in contrast to the structure of the "blue box" (**1**) in which the bipyridinium residues lie essentially perpendicular to the mean plane of the macrocycle.[32]

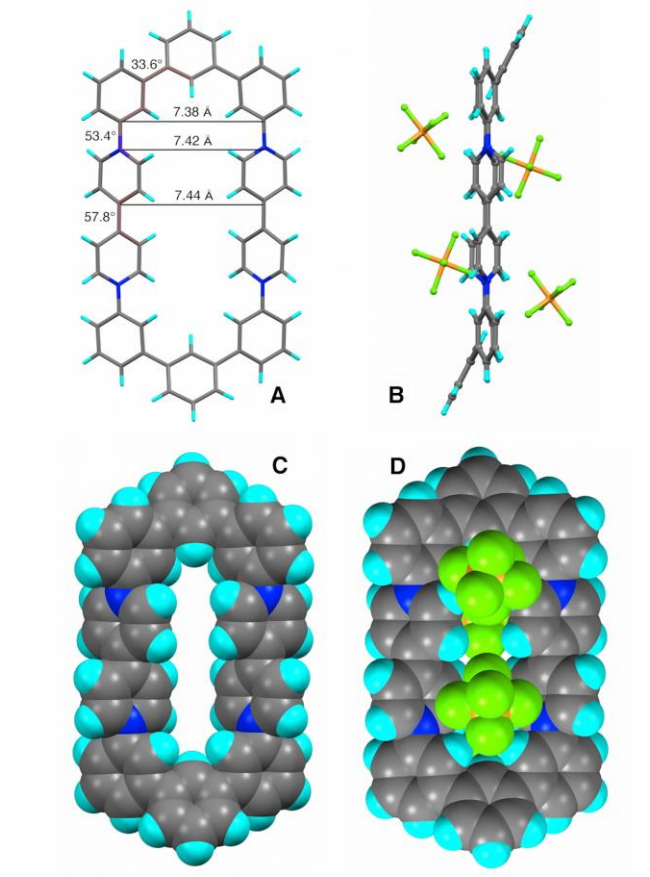

Fig. 2 Molecular structure of macrocycle $\mathbf{4}^{4+}$ as its hexafluorophosphate salt. (A) Inter-ring torsion angles and inter-annular distances. (B) Close contacts between the macrocycle and its associated anions in the crystal. (C) Space filling representation of the macrocycle, showing how the 4,4'-bipyridinium rings rotate to self-fill the macrocyclic cavity. (D) space-filling representation of the crystal structure showing how the hexafluorophosphate anions associate with the cationic macrocycle.

Thus, even though the transannular atom–atom distances in $\mathbf{4}^{4+}$ (Figure 2A) show a clear potential for binding aromatic guests, complexation requires a conformational reorganisation involving rotation of the 4,4'-bipyridinium rings away from the macrocyclic plane. In the crystal, each tetracationic macrocycle is closely associated with four hexafluorophosphate anions, two above and two below the plane (Figures 2B and 2D), and all four anions also interact edge-on with neighbouring macrocycles. If such ion-pairing were to be carried over to the solution phase, complexation of an aromatic guest molecule would require a further structural rearrangement involving displacement of $[PF_6]^-$ anions from the cationic macrocycle.

The chemical stability and reversible redox reactivity of the macrocycle were studied by addition of an excess of the nucleophile/electron-donor triethylamine (TEA), followed by trifluoroacetic acid (TFA). Figure 3(A) shows the ^{1}H NMR spectrum of the pale-yellow solution of macrocycle $\mathbf{4}^{4+}$, which exhibits clearly resolved signals in the aromatic region (7.5 to 10.0 ppm). On addition of TEA, *all* the signals corresponding to the protons of the aromatic and heterocyclic rings disappear (Figure 3(B)) because of extreme line broadening. This result indicates the formation of $\mathbf{4}^{2(\bullet+)}$ that would be expected to be paramagnetic as a result of being a bis(radical cation). The transformation of the ^{1}H NMR spectrum is accompanied by the solution turning deep green, a colour which indicates the presence of the viologen radical-cationic chromophore.[63] Addition of an excess of TFA to this system led to the recovery of the original colour of the solution and reappearance of the ^{1}H NMR signals of diamagnetic macrocycle $\mathbf{4}^{4+}$ (Figure 3C).

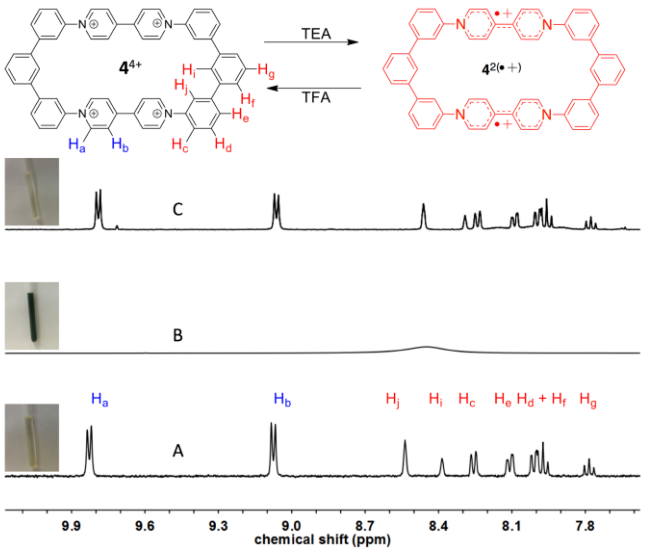

Fig. 3 Chemical reduction and reoxidation of $\mathbf{4}^{4+}$ using TEA and TFA, respectively. The figure shows ^{1}H NMR spectra and photographs of the following samples: (A) **1** in acetonitrile-d_3, (B) after addition of TEA, forming the bis(radical cation) $\mathbf{4}^{2(\bullet+)}$ and (C) following addition of an excess of TFA to B to regenerate $\mathbf{4}^{4+}$. The loss of all proton signals in spectrum B indicates that under these conditions, i.e., in the presence of TEA radical cations ($TEA^{\bullet+}$), the single electron spin density is not only located across the 4,4'-bipyridinium rings (see the DFT section) but also affects the whole macrocycle (spin exchange).

The cyclic voltammogram (CV) and square wave voltammogram (SWV) of compound $\mathbf{4}^{4+}$ are shown in Figure 4. Two well-resolved bielectronic cathodic waves are observed for the macrocycle at $E_{1/2}$ = -0.65 and -0.97 V vs Fc/Fc^+. These signals correspond to the initial reduction of the parent tetracationic species ($\mathbf{4}^{4+}$) to the stable bis(radical cation) ($\mathbf{4}^{2(\bullet+)}$) and then to the neutral, quinoidal species (**4**). Both redox couples are fully reversible under these conditions.

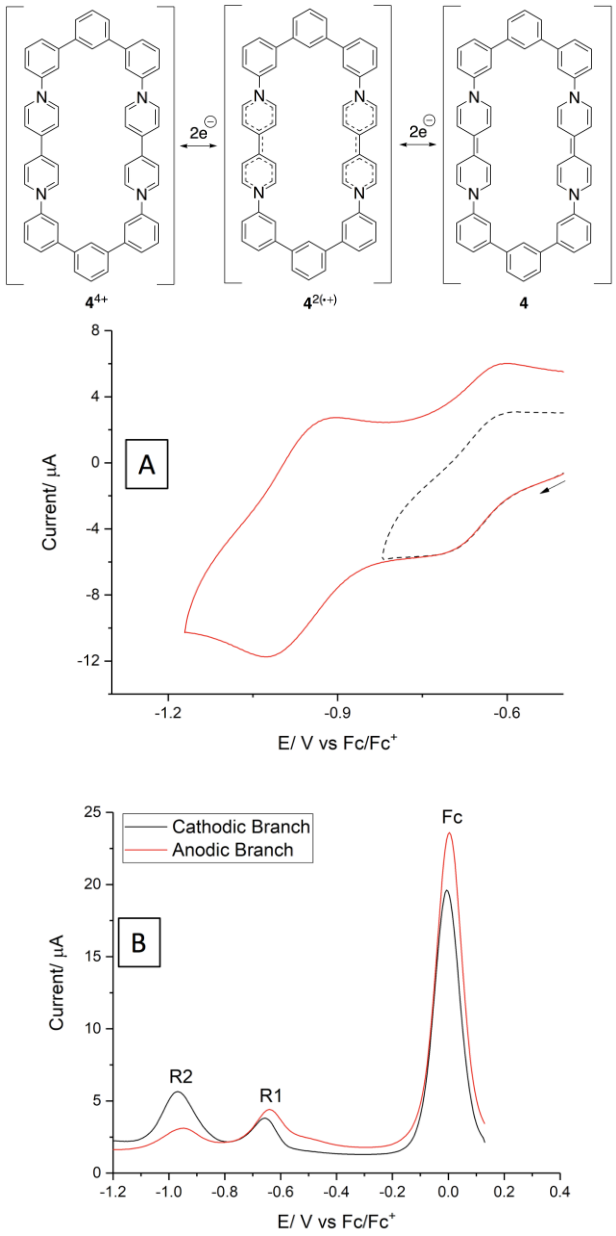

Fig. 4 Structures of the bis(radical cationic) $4^{2(\bullet+)}$ and neutral, quinoidal species **4** formed by the two-step electrochemical reduction of 4^{4+}, as reflected in the corresponding CV and SWV responses (voltammograms (A) and (B), respectively). Voltammograms were recorded for $2 \cdot 10^{-4}$ M 4^{4+} at a glassy carbon disc (d = 2 mm) electrode in anhydrous, degassed DMF/10^{-1} M TBAH. The arrow indicates the initial potential sweep direction. Scan parameters: cyclic voltamemtry (CV) - v = 0.5 V s^{-1}; square-wave voltammetry (SWV) - f = 25 Hz and t_p = 20 mV.

UV-Vis spectroelectrochemistry (SEC) was carried out at 293 K with $2 \cdot 10^{-4}$ M 4^{4+} in MeCN/10^{-1} M tetra-*n*-butylammonium hexafluorophosphate (TBAH) in an OTTLE cell.[64] Conversion of the tetracationic species to the bis(radical cation) results in depleted absorbance at 315 nm and concurrent appearance of new absorption bands at 430, 585, 640 and 710 nm (Figure 5A). These spectral changes in the visible region are consistent with the formation of a viologen radical cation.[65] The isosbestic point at 365 nm reveals the stability of $4^{2(\bullet+)}$ on the timescale of the experiment. Further cathodic potential sweep towards the reduction of $4^{2(\bullet+)}$ resulted in a further increase and slight red shift of the absorption near 445 nm together with the disappearance of the composed absorption between 550-750 nm, suggesting the formation of the neutral, quinoid form of the macrocycle (**4**).[48,49] The second cathodic step, however, was not completed under the experimental conditions, most likely as a consequence of working electrode passivation in the acetonitrile electrolyte (as also revealed by cyclic voltammetry).

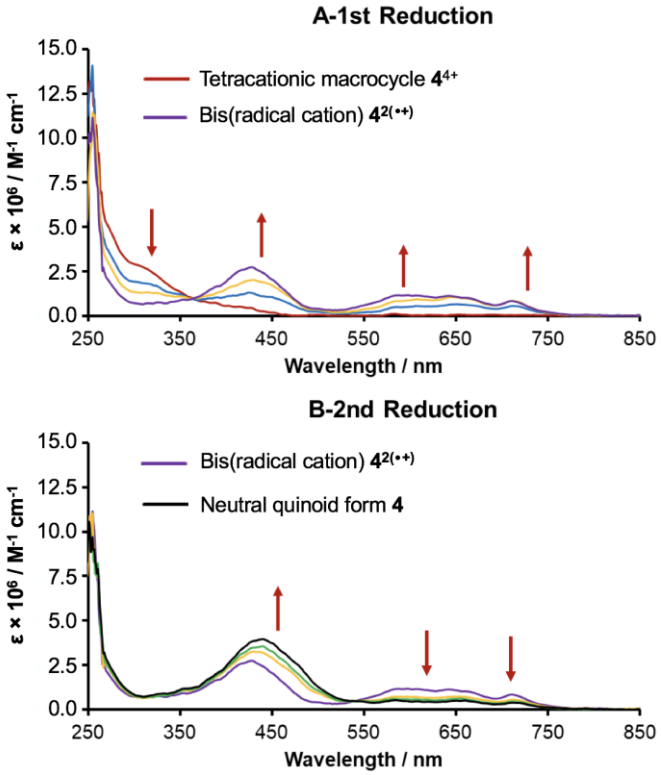

Fig. 5 UV-vis spectral changes accompanying the stepwise electrochemical reduction of macrocycle 4^{4+} to bis(radical cation) $4^{2(\bullet+)}$ (spectral set A) and the neutral quinoid form, **4** (spectral set B) in anhydrous MeCN/10^{-1} M TBAH, using an OTTLE cell.[64]

Quantum chemical calculations on the electronic structures of the three discrete redox states of the macrocycle

Density functional theory (DFT) geometry optimization studies of 4^{4+}, $4^{2(\bullet+)}$ and **4** were performed for singlet, triplet, and singlet states, respectively. Both bond lengths and geometries derived from the results of the *in vacuo* DFT calculations for 4^{4+} are in good agreement with those observed in the crystal structure of the macrocycle (see SI Table S1 for full comparison).

DFT studies including solvent interactions for the three oxidation states of the macrocycle were also conducted. The most significant differences in bond lengths and geometries between the structures occurs within the viologen residues of the macrocycle (see SI Table 2 for complete data). Inspection of the calculated LUMO of 4^{4+} and spin density distribution in triplet $4^{2(\bullet+)}$ (Figure 6) reveals the dominant involvement of the viologen rings in the bielectronic reduction step. In addition, the twisted conformations of the viologen residues in their parent dicationic forms (Fig. 6A) are significantly reduced in the bis(radical cation) form of the macrocycle (6B). This conformational reorganisation within viologen species on reduction has been observed in the crystal structures of related species.[25,47] However, the localisation of the spin density within the heterocyclic rings in the bis(radical cation) form of the macrocycle results in little change in the bond lengths of the *m*-

terphenyl groups between the $\mathbf{4}^{4+}$ and $\mathbf{4}^{2(\bullet+)}$ oxidation states (see SI Table S2 for complete data). This suggests that under the electrochemical reduction conditions, the unpaired electron density is only weakly delocalised over the adjacent *m*-terphenyl rings, in non-bonding orbital combinations (Fig.6).

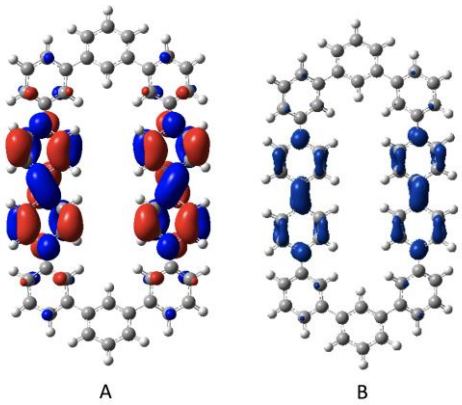

Fig. 6 The calculated lowest unoccupied molecular orbital (LUMO) of $\mathbf{4}^{4+}$ (A), and spin density distribution in $\mathbf{4}^{2(\bullet+)}$ (B). Note the twist in the bond between the pyridinium residues in $\mathbf{4}^{4+}$ compared to the relatively planar orientation of the heterocyclic rings in $\mathbf{4}^{2(\bullet+)}$.

The UV-vis electronic transitions for the three oxidation states of the macrocycle were calculated using time dependent (TD) DFT methods. The simulated UV-vis spectra for these species are presented in Fig. 7. The calculated absorption maxima and relative intensities for each oxidation state are in good agreement with the experimental UV-vis spectroelectro-chemical data (Table 1). This provides further evidence for validity of the calculated orbitals for all three of these oxidation states and, therefore, the localization of the unpaired spin electron density on the radical cationic viologen residues in $\mathbf{4}^{2(\bullet+)}$. The lowest-energy electronic transitions in for each oxidation state are and visualised in Supporting Information, Figures S1 ($\mathbf{4}^{4+}$), S2 ($\mathbf{4}^{2(\bullet+)}$) and S3 (**4**). The electronic absorption of $\mathbf{4}^{2(\bullet+)}$ was analysed in a greater detail; the calculated vertical excitations with oscillator strength above 0.005 are presented in Table S3 and Figure S4. The corresponding α- and β-spinorbitals involved are visualised in Figures S5 and S6, respectively.

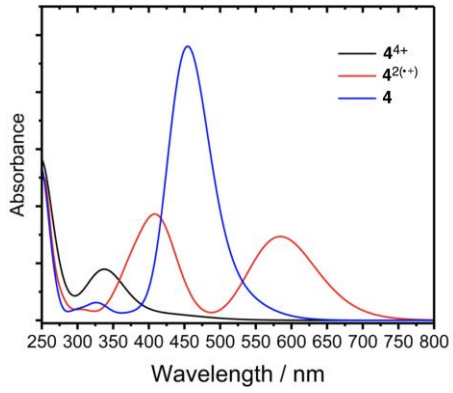

Fig. 7 Calculated electronic absorption spectra for the three oxidation states of the macrocycle.

Table 1 Experimental and calculated data peak maxima for each oxidation state of the macrocycle

Macrocycle oxidation state		λ [nm]
$\mathbf{4}^{4+}$	Experimental	315
	Calculated	339[b]
$\mathbf{4}^{2(\bullet+)}$	Experimental	430, 585 (640, 720)
	Calculated[a]	416, 584[c]
4	Experimental	445
	Calculated	453[d]

[a]Detailed analysis is presented in SI Table S3, [b]See SI Figure S1; [c] See SI Figure S2; [d] See SI Figure S3

Macrocycle Binding Studies

The binding properties of macrocycle $\mathbf{4}^{4+}$ were investigated by ^{1}H NMR spectroscopy. In the course of the experiment, $\mathbf{4}^{4+}$ was titrated with the π-electron-rich guest molecule **10** (Figure 8).[66] As a result, the signals of H_a and H_b on the 4,4-bipyridinium units of $\mathbf{4}^{4+}$ underwent significant (0.25 ppm) complexation-induced, upfield shifts. This behaviour indicates an exposure of the protons to ring-current shielding by one or more naphthalene rings of **10**. Conversely, a small, but measurable (0.05 ppm) downfield shift in the resonance frequency of the protons H_i points to their location within the ring-current *de*shielding torus generated by the aromatic π-systems of **10**. These shielding and deshielding effects are consistent with a structure where a 1,5-dioxonaphthalene unit is encapsulated within the macrocycle, stacking face-to-face with the bipyridinium residues, as observed for related systems.[46,47] The binding constant of 150 ± 30 M^{-1} was determined from the ^{1}H NMR titration data using the program *Bindfit*.[67]

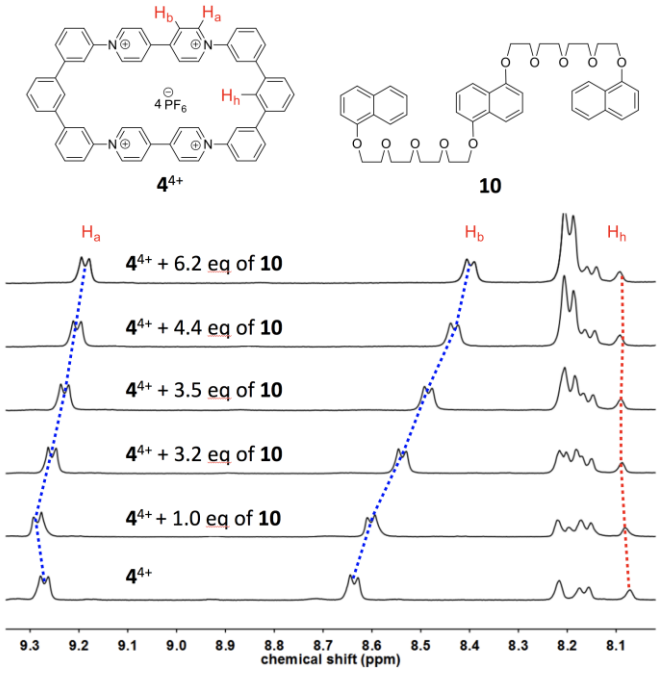

Fig. 8 ^{1}H NMR (400 MHz) spectral changes induced by titration of macrocycle $\mathbf{4}^{4+}$ with the guest species **10** in CD_3CN at 298 K.

Diffusion ^{1}H NMR experiments further confirmed the successful complexation of **10** with macrocycle $\mathbf{4}^{4+}$ (Figure 9). The diffusion coefficient of a species can be estimated using the Stokes-Einstein equation,[68–71] with an inverse relationship between the molecular size and diffusion coefficient. The measured diffusion coefficient of a molecule, when binding with another, is a weighted average of the diffusion coefficients of the free molecule and that observed when bound.[72] In this case, the insertion of the guest molecule into the cavity in the macrocycle leads to only a small increase in size, as the macrocycle $\mathbf{4}^{4+}$ (D = 7.25×10^{-10} m^2 s^{-1} in acetonitrile, in the absence of **10**) is already larger than **10** (D = 8.0×10^{-10} m^2 s^{-1} in acetonitrile, in the absence of $\mathbf{4}^{4+}$).

Using only signals from 4,4-bipyridinium (H_a and H_b, Figure 6), to avoid complications due to overlapping signals, diffusion coefficients of 1.25 mM the macrocycle ($\mathbf{4}^{4+}$) were measured in the presence of 0, 1.3, 2.6 and 13 mM of guest molecule **10**. The diffusion coefficient of the macrocycle was observed to decrease with increasing concentration of guest, as shown in Figure 7, indicating binding of the two molecules to form a larger complex. Some saturation of the interaction was observed when a large excess of guest was added (See SI Fig S7 for DOSY spectra). Thus, despite an initially unfavourable conformation (Figure 2), macrocycle $\mathbf{4}^{4+}$ can clearly re-orient its 4,4'-bipyridinium residues to allow binding of aromatic guests within the cavity.

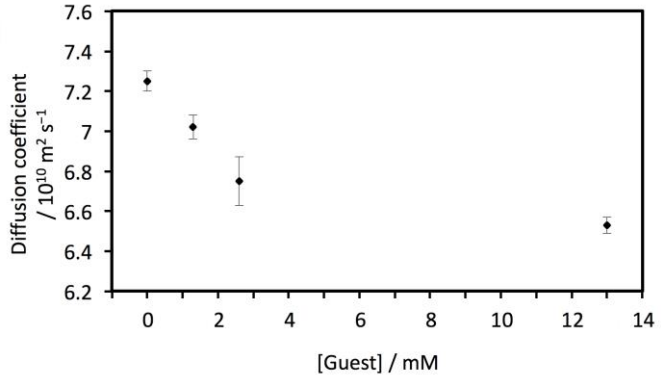

Fig. 9 Diffusion coefficients for macrocycle $\mathbf{4}^{4+}$ ($1.25 \cdot 10^{-3}$ M, CD_3CN) measured in the presence of guest **10** (0 – $1.3 \cdot 10^{-3}$ M).

Conclusions

A novel, di(viologen) macrocyclic receptor molecule containing fully conjugated linker groups has been designed, synthesised, and characterised. The transannular N…N bond distance is approximately 7.4 Å, as determined by single-crystal X-ray diffraction. Addition of NEt_3 to tetracation $\mathbf{4}^{4+}$ results in its reduction to a green bis(radical cationic) species ($\mathbf{4}^{2(\bullet+)}$), which can be re-oxidised to the parent macrocycle ($\mathbf{4}^{4+}$) by addition of TFA. Macrocycle $\mathbf{4}^{4+}$ undergoes two reversible 2-electron reduction processes which ultimately result in the formation of a neutral form of the parent macrocycle. DFT studies accurately model both the solid-state structure of $\mathbf{4}^{4+}$ and the electronic absorption spectra of each of the three oxidation states. The calculations reveal that the unpaired electron density in $\mathbf{4}^{2(\bullet+)}$ is largely confined to the heterocyclic rings in the macrocycle. Complexation studies were carried out by the addition of the π-electron rich species **10** to $\mathbf{4}^{4+}$. Analysis of 1D ^{1}H NMR and DOSY data were fully consistent with the formation of a pseudorotaxane-type complex where a naphthalene residue of the guest molecule was positioned in the cavity of the macrocycle. The complex formed with an association constant of 150 M^{-1} (± 30 M^{-1}).

Experimental

General methods: Starting materials were purchased from Sigma Aldrich and Alfa Aesar and used without further purification, unless otherwise stated. Anhydrous *N*,*N*-dimethylformamide (DMF) (Alfa Aesar, 99.8%, packaged under argon) was used as received. Tetra-*n*-butylammonium hexafluorophosphate (TBAH) was recrystallized twice from absolute ethanol and dried at 80 °C under vacuum overnight.

Compounds **8** and **9** were synthesized as described previously.[46,61] All reactions were carried out in oven-dried glassware under dry nitrogen.

^{1}H and ^{13}C NMR spectra were acquired on a Bruker DPX-400 spectrometer operating at 400 MHz and 100 MHz respectively. Residual ^{1}H signals of the solvent were used as internal calibrants. Infrared spectra were recorded on a Perkin Elmer 17 20-X spectrometer, using thin films cast from acetone, and major absorption bands are reported in wavenumbers (cm^{-1}).

Spectroelectrochemical measurements were carried out at 293 K, using an optically transparent thin-layer electrochemical (OTTLE) cell equipped with Pt minigrid working and auxiliary electrodes, a silver microwire pseudoreference electrode, and CaF_2 windows. The course of the spectroelectrochemical experiment was monitored by thin-layer cyclic voltammetry with an EmStat3 (PalmSens BV) potentiostat. Cyclic voltammetric (CV) measurements were performed on $2 \cdot 10^{-4}$ M mM solutions of compound $\mathbf{4}^{4+}$ in anhydrous, degassed DMF containing 10^{-3} M TBAH as the supporting electrolyte, with a single-compartment three-electrode cell equipped with a carefully polished glassy carbon disc (d = 2 mm) working electrode, coiled platinum wire auxiliary and coiled silver wire pseudoreference electrodes.

Melting points were determined as the peak maximum of a DSC thermogram acquired on a TA Instruments DSC Q2000. Mass spectra were recorded on a Bruker MicroTOF QII instrument using electrospray ionisation.

Diffusion-ordered (DOSY) NMR: Samples containing 2.5 mM of $\mathbf{4}^{4+}$ and 0, 1.3, 2.6 and 13 mM of **10** were prepared in CD_3CN. Measurements were carried out with non-spinning samples on a 300 MHz Bruker Avance spectrometer, using a 5 mm PABBO BB-1H ZGRD probe equipped with a z-gradient coil producing a maximum gradient of 36 G cm^{-1}. All NMR measurements were made at constant temperature (22 ± 0.5 °C) and used the double-stimulated echo bipolar pulse pair sequence[73] (DSTEBPGP_3S in the Bruker library, with an additional gradient added to balance the 3 spoil gradients), to remove from the diffusion measurements any possible effects of convection.[74,75] Proton spectra were acquired with a single scan of 16384 complex data points. Diffusion data were acquired with ten magnetic field gradient amplitudes ranging from 28.7 to 7.2 G cm^{-1}, incremented in equal steps of gradient squared. For each gradient amplitude, 128 transients of 16384 complex data points were acquired for a total experimental time of 1 h 55 min. The diffusion delay time, Δ, was set to 0.12 s to obtain *ca*.

80% attenuation of signals. The gradient encoding time for all experiments was 1 ms and all gradients were half-sine in shape. Diffusion coefficients and DOSY spectra were then estimated and produced using the DOSY Toolbox software package.[76]

A crystal of $\mathbf{4}^{4+}$ was mounted under Paratone-N oil and flash cooled to 150 K in a stream of nitrogen in an Oxford Cryostream cooler. Single-crystal X-ray intensity data were collected using an Agilent Gemini S Ultra diffractometer (Mo Kα radiation (λ = 0.71073 Å)). The data were reduced within the CrysAlisPro software.[77] The structure was solved using the program Superflip[78] and all non-hydrogen atoms were located. Least-square refinements on *F* were carried out using the CRYSTALS suite of programs.[79] The non-hydrogen atoms were refined anisotropically. Each hydrogen atom of the ligands was placed geometrically with a C-H distance of 0.95 Å and a U_{iso} of 1.2-1.5 times the value of U_{iso} of the parent C atom.

There was disordered solvent within the structure which could not be modelled satisfactorily. The PLATON SQUEEZE software enabled the contribution to diffraction of the 4 disordered solvent molecules per asymmetric unit (i.e., 2 CH_3CN + 2 Et_2O) to be calculated and, thus, it was possible to produce solvent-free diffraction intensities.[77–80] The data have been deposited at the CCDC (code CCDC 1828538).

The electronic structures of $\mathbf{4}^{4+}$, $\mathbf{4}^{2(\bullet+)}$ and **4** were calculated by density functional theory (DFT) methods using the Gaussian 09 (G09)[81] program package. Geometry optimization followed by vibrational analysis was made either in vacuum or in solvent media. G09 calculations employed Perdew, Burke, Ernzerhof[82,83] PBE0 hybrid functional (G09/PBE0) together with Grimme's dispersion correction GD3BJ[84]. Polarized triple- ζ basis sets 6-311G(d) for all atoms were used.[85,86] Solvent effects were described by the polarizable continuum model (PCM).[87] Electronic transitions were calculated by time-dependent DFT (TD-DFT) method at optimized geometries.

Synthesis of 3,3"-diamino-*m*-terphenyl 3 (ref.[57])**:** A solution of palladium(II) acetate (50 mg, 2 mmol) and intermediate (**7**) (1.30 g, 4 mmol) in tetrahydrofuran (20 mL) was stirred until homogeneous. A solution of potassium fluoride (1 g, 17.2 mmol) in water (8 mL) was added to the solution, and liquid polymethylhydrosiloxane (4 mL, 32 mmol) was then added dropwise. The solution was stirred for 3 h. Chloroform (100 mL) was added to the reaction mixture and the organic phase was separated and concentrated under vacuum. The resulting oil was easily purified by column chromatography on silica gel (ethanol: hexane 1:4, v/v) to afford the desired diamine as yellow oil (0.83 g, 100%). ^{1}H NMR (DMSO-d_6, 400 MHz) δ (ppm) 7.58 (s, 1H), 7.39 (m, 3H), 7.01 (t, *J* = 7.02, 2H), 6.79 (s, 2H), 6.72 (d, J = 6.7, 2H), 6.47 (d, *J* = 6.5, 2H) 5.06 (s, 2NH_2); ^{13}C NMR (DMSO-d_6, 100 MHz) δ 149.1, 141.5, 140.9, 129.4, 129.1, 125.2, 124.6, 114.4, 113.2, 112.2; IR (cm^{-1}) $\bar{\upsilon}$ = 3367 (N-H) 1598 (N–H bend), 1478 (C–N), 907 (N–H wag). MS (*m*/*z*) calc. for $(C_{18}H_{17}N_2)^+$: 261.1392, found 261.1384.

Synthesis of tetracationic macrocycle $\mathbf{4}^{4+}$ (1,2,7(4,1),6(1,4)-tetrapyridin-1-iuma-3,4,5,8,9,10(1,3)-hexabenzena-cyclo-decaphane-11,21,61,71-tetraium tetrakis (hexafluorophosphate): A solution of Zincke salt (**8**) (431 mg, 0.768 mmol) in a mixture of EtOH (3 mL) and water (2 mL) and a solution of aromatic diamine (**3**) (200 mg, 0.768 mmol) in DMAc (5 mL) were added drop-wise to a rapidly stirred DMAc 80 mL) at 50 °C *via* two syringes. The reaction mixture was stirred under a positive pressure of argon for 5 d. After cooling to room temperature, the solution was concentrated to approximately 5 mL under reduced pressure and added slowly to a rapidly stirred solution of NH_4PF_6 (20 g) in water (200 ml). After stirring at room temperature for 1 h, the resulting yellow precipitate was collected by filtration, washed with water (2 × 20 mL) and dried in vacuo overnight. Purification was achieved by crystallisation from a mixture of acetonitrile and acetone (10:90, v/v) to afford macrocycle **1** as a yellow solid (100 mg, 10%). M.p. 216-218 °C. ^{1}H NMR acetone-d_6, 400 MHz) δ 9.83 (d, *J* = 6.7 Hz, 4H), 9.08 (d, *J* = 6.7 Hz, 4H), 8.54 (s, 4H), 8.39 (s, 2H), 8.26 (d, *J* = 7.5 Hz, 4H), 8.11 (d, *J* = 6.6 Hz, 4H), 8.05 – 7.91 (m, 6H), 7.78 (t, *J* = 7.7 Hz, 2H). ^{13}C NMR (acetonitrile-d_3, 100 MHz) δ 150.4, 145.5, 142.8, 142.4, 139.0, 130.9, 130.2, 127.2, 127.0, 125.4, 123.4, 123.1. MS (*m*/*z*) calc. for $(C_{56}H_{40}N_4F_{12}P_2)^{2+}$: 529.1263, found 529.1263.

Synthesis of 3,3"-dinitro-*m*-terphenyl 7 (ref.[57])**:** 3-Dibromobenzene (1.5 g, 6.36 mmol), 3-nitrophenyl boronic acid (**5**, 2.23 g, 13.3 mmol), Na_2CO_3 (2.7 g, 25.4 mmol), and $Pd(OAc)_2$ (～15 mg), were stirred in a mixture of water (30 mL) and DMF (55 mL) at 70 °C overnight. The product was precipitated in water, filtered off and washed with methanol, then water, then methanol once again before drying under vacuum for 2 h to afford the dinitro-intermediate (**7**) as a grey powder (1.54 g, 66.5%). M.p. (DSC) 210 °C; ^{1}H NMR (DMSO-d_6, 400 MHz) δ 8.59 (s, 2H), 8.30 (d, *J* = 7.6, 2H), 8.28 (d, *J* = 8.0, 2H), 8.16 (s, 1H), 7.86 (d, *J* = 8.0, 2H) 7.79 (t, *J* = 8.4, 2H) 7.67 (t, *J* = 7.6, 1H); ^{13}C NMR (DMSO-d_6, 100 MHz) δ (ppm) 148.5, 141.4, 138.8, 133.7, 130.4, 130.1, 127.3, 125.9, 122.36, 121.8; IR (cm^{-1}) $\bar{\upsilon}$ = 1528 (N–O), 1344 (C–N), 888 (C–H Ar). MS (*m*/*z*) calc. for $(C_{18}H_{12}N_2O_4)^+$: 320.0797, found 320.0799.

Synthesis of 10: 1-naphthol (905 mg, 6.28 mmol) was placed in a dry round bottomed flask with dry acetonitrile under argon. Potassium carbonate (427 mg, 3.09 mmol) and 18-crown-6 (100 mg, 0.5 mmol) were added to the solution and it was heated under reflux for 1 h before the ditosylate (**11**) (984 mg, 1.68 mmol) was added. The reaction mixture was heated at reflux under argon for further 2 d. The solvent was evaporated under reduced pressure, the residue was washed with H_2O, and then finally extracted into CH_2Cl_2 and dried under high vacuum overnight to yield **10** as an orange oil (2.36 g, 100%). ^{1}H NMR ($CDCl_3$, 400 MHz) δ 8.27 (d, *J* = 6.6 Hz, 2H), 7.85 (d, *J* = 8.2 Hz, 2H), 7.77 (d, *J* = 6.8 Hz, 2H), 7.45 – 7.40 (m, 2H), 7.32 (dd, *J* = 16.5, 8.2 Hz, 4H), 6.77 (d, *J* = 7.2 Hz, 4H), 4.25 – 4.23 (m, 8H), 3.96 (d, *J* = 1.9 Hz, 8H), 3.74 (d, *J* = 26.1 Hz, 16H). ^{13}C NMR ($CDCl_3$, 100 MHz) δ 154.5, 154.3, 134.5, 127.4, 126.4, 125.8, 125.1, 122.1, 120.4, 114.6, 105.6, 104.9, 70.9, 70.7, 69.8, 67.8, 67.8. MS (*m*/*z*) calc. for $(C_{46}H_{53}O_{10})^{2+}$: 765.3633, found 765.3633.

Synthesis of ditosylate 11: Triethylamine (Et_3N, 2.1 g, 20.8 mmol) and *N,N'*-dimethylaminopyridine (DMAP) (0.854 g, 6.91 mmol) were added to a solution of **9** (4.03 g, 7.5 mmol) in dry CH_2Cl_2 (175 mL) at 0 °C under a nitrogen atmosphere. After 5 min, a solution of TsCl (4.0 g, 21.2 mmol) was added directly to the reaction. The reaction mixture was allowed to warm up to room temperature and stirred for another 12 h. The solvent was removed, washed with H_2O, extracted with EtOAc and DCM. The organic layers were combined and dried with $MgSO_4$, the solvent was removed to yield the crude product. Purification was achieved by precipitation with acetone and petroleum

ether (40-60 °C) **11** as a yellow oil (3.24 g, 57%). ^{1}H NMR ($CDCl_3$, 400 MHz) δ 7.85 (d, *J* = 8.5 Hz, 2H), 7.35-7.29 (m, 6H), 6.84 (d, *J* = 7.6 Hz, 2H), 4.29 (t, *J* =4.7 Hz, 4H), 4.13(t, *J* = 4.8 Hz, 4H), 3.99 (t, *J* = 5.0 Hz, 4H), 3.79-3.77 (m, 4H), 3.67-3.64 (m, 8H), 3.61-3.55 (m, 8H), 2.41 (s, 6H). (Data in agreement with ref.[60])

Notes

The authors declare no competing financial interests.

Acknowledgements

We thank the University of Reading for access to the CAF lab. Spectroelectrochemistry Reading laboratory (spinout) supported this project.

Notes and References:

1 J.-M. Lehn, *Angew. Chem. Int. Ed.*, 1988, **27**, 89–112.
2 E. R. Kay, D. A. Leigh and F. Zerbetto, *Angew. Chem. Int. Ed.*, 2007, **46**, 72–191.
3 L. Fang, M. A. Olson, D. Benítez, E. Tkatchouk, W. A. Goddard III and J. F. Stoddart, *Chem. Soc. Rev.*, 2010, **39**, 17–29.
4 C. Cheng, P. R. McGonigal, J. F. Stoddart and R. D. Astumian, *ACS Nano*, 2015, **9**, 8672–8688.
5 C. Pezzato, C. Cheng, J. F. Stoddart and R. D. Astumian, *Chem. Soc. Rev.*, 2017, **46**, 5491–5507.
6 M. M. Boyle, R. A. Smaldone, A. C. Whalley, M. W. Ambrogio, Y. Y. Botros and J. F. Stoddart, *Chem. Sci.*, 2011, **2**, 204–210.
7 T. van Leeuwen, A. S. Lubbe, P. Štacko, S. J. Wezenberg and B. L. Feringa, *Nat. Rev. Chem.*, 2017, **1**, 96.
8 W. R. Browne and B. L. Feringa, *Nat. Nanotechnol.*, 2006, **1**, 25–35.
9 P. M. S. Monk, *The Viologens: Physiochemical Properties, Synthesis and Applications of Salts of 4,4'-Bipyridine*, Wiley, 1998.
10 J. F. Stoddart and H. M. Colquhoun, *Tetrahedron*, 2008, **64**, 8231–8263.
11 J. F. Stoddart, *Chem. Soc. Rev.*, 2009, **38**, 1802.
12 Y. Wang, M. Frasconi and J. F. Stoddart, *ACS Cent. Sci.*, 2017, **3**, 927–935.
13 D. W. Zhang, J. Tian, L. Chen, L. Zhang and Z. T. Li, *Chem. Asian J.*, 2015, **10**, 56–68.
14 J. M. Spruell, *Pure Appl. Chem.*, 2010, **82**, 2281–2294.
15 M. Berville, L. Karmazin, J. A. Wytko and J. Weiss, *Chem. Commun.*, 2015, **51**, 15772–15775.
16 S. Ahmed, N. Singha, B. Pramanik, J. H. Mondal and D. Das, *Polym. Chem.*, 2016, **7**, 4393–4401.
17 Y. Wang, M. Frasconi, W. G. Liu, J. Sun, Y. Wu, M. S. Nassar, Y. Y. Botros, W. A. Goddard, M. R. Wasielewski and J. F. Stoddart, *ACS Cent. Sci.*, 2016, **2**, 89–98.
18 A. C. Fahrenbach, J. C. Barnes, D. A. Lanfranchi, H. Li, A. Coskun, J. J. Gassensmith, Z. Liu, D. Benítez, A. Trabolsi, W. A. Goddard, M. Elhabiri and J. F. Stoddart, *J. Am. Chem. Soc.*, 2012, **134**, 3061–3072.
19 C. Cheng, P. R. McGonigal, S. T. Schneebeli, H. Li, N. A. Vermeulen, C. Ke and J. F. Stoddart, *Nat. Nanotechnol.*, 2015, **10**, 547–553.
20 G. J. Ashwell, G. H. Cross, D. A. Kennedy and I. W. Nowell, *J. Chem. Soc. Perkin Trans . II*, 1983, 1787–1791.
21 G. J. Ashwell and J. G. Allen, *J. Phys. Colloq.*, 1983, **44**, 1261–1264.
22 G. J. Ashwell, J. G. Allen, E. P. Goodings and I. W. Nowell, *Cryst. Struct. Electr. Conduct.*, 1984, **82**, 301–306.
23 D. R. Rosseinsky and P. M. S. Monk, *J. Chem. Soc., Faraday Trans.*, 1994, **90**, 1127–1131.
24 W. W. Porter and T. P. Vaid, *J. Org. Chem.*, 2005, **70**, 5028–5035.
25 W. W. Porter and T. P. Vaid, *J. Mater. Chem.*, 2007, **17**, 469.
26 N. Leblanc, N. Mercier, O. Toma, A. H. Kassiba, L. Zorina, P. Auban-Senzier and C. Pasquier, *Chem. Commun.*, 2013, **49**, 10272.
27 A. C. Fahrenbach, S. Sampath, D. J. Late, J. C. Barnes, S. L. Kleinman, N. Valley, K. J. Hartlieb, Z. Liu, V. P. Dravid, G. C. Schatz, R. P. Van Duyne and J. F. Stoddart, *ACS Nano*, 2012, **6**, 9964–9971.
28 M. Lee, U. H. Choi, R. H. Colby and H. W. Gibson, *Macromol. Chem. Phys.*, 2015, **216**, 344–349.
29 B. Odell, M. V. Reddington, A. M. Z. Slawin, N. Spencer, J. F. Stoddart and D. J. Williams, *Angew. Chem. Int. Ed.*, 1988, **11**, 1547–1550.
30 J. C. Barnes, M. Juríček, N. L. Strutt, M. Frasconi, S. Sampath, M. A. Giesener, P. L. McGrier, C. J. Bruns, C. L. Stern, A. A. Sarjeant and J. F. Stoddart, *J. Am. Chem. Soc.*, 2013, **135**, 183–192.
31 M. Juríček, J. C. Barnes, E. J. Dale, W. G. Liu, N. L. Strutt, C. J. Bruns, N. A. Vermeulen, K. C. Ghooray, A. A. Sarjeant, C. L. Stern, Y. Y. Botros, W. A. Goddard and J. F. Stoddart, *J. Am. Chem. Soc.*, 2013, **135**, 12736–12746.
32 J. C. Barnes, M. Juríček, N. A. Vermeulen, E. J. Dale and J. F. Stoddart, *J. Org. Chem.*, 2013, **78**, 11962–11969.
33 E. J. Dale, D. P. Ferris, N. A. Vermeulen, J. J. Henkelis, I. Popovs, M. Juríček, J. C. Barnes, S. T. Schneebeli and J. F. Stoddart, *J. Am. Chem. Soc.*, 2016, **138**, 3667–3670.
34 J. Sun, M. Frasconi, Z. Liu, J. C. Barnes, Y. Wang, D. Chen, C. L. Stern and J. F. Stoddart, *Chem. Commun.*, 2015, **51**, 1432–1435.
35 G. Barin, A. Coskun, M. M. G. Fouda and J. F. Stoddart, *ChemPlusChem*, 2012, **77**, 159–185.
36 H. M. Colquhoun, D. J. Williams and Z. Zhu, *J. Am. Chem. Soc.*, 2002, **124**, 13346–13347.
37 S. C. Zimmerman, M. Mrksich and M. Baloga, *J. Am. Chem. Soc.*, 1989, **111**, 8528–8530.
38 Z. Zhu, C. J. Cardin, Y. Gan and H. M. Colquhoun, *Nat. Chem.*, 2010, **2**, 653–660.
39 B. W. Greenland, M. B. Bird, S. Burattini, R. Cramer, R. K. O'Reilly, J. P. Patterson, W. Hayes, C. J. Cardin and H. M. Colquhoun, *Chem. Commun.*, 2013, **49**, 454–456.
40 F. B. L. Cougnon, H. Y. Au-Yeung, G. D. Pantoş and J. K. M. Sanders, *J. Am. Chem. Soc.*, 2011, **133**, 3198–3207.
41 D. Philp, A. M. Z. Slawin, N. Spencer, J. F. Stoddart and D. J. Williams, *J. Chem. Soc., Chem. Commun.*, 1991, 1584–1586.
42 C. A. Hunter and J. K. M. Sanders, *J. Am. Chem. Soc.*, 1990, **112**, 5525–5534.
43 C. R. Martinez and B. L. Iverson, *Chem. Sci.*, 2012, **3**, 2191.
44 O. S. Miljanic and J. F. Stoddart, *Proc. Nat. Acad. Sci.*, 2007, **104**, 12966–12970.
45 J. M. Spruell, W. R. Dichtel, J. R. Heath and J. F. Stoddart, *Chem. Eur. J.*, 2008, **14**, 4168–4177.
46 H. M. Colquhoun, B. W. Greenland, Z. Zhu, J. S. Shaw, C. J. Cardin, S. Burattini, J. M. Elliott, S. Basu, T. B. Gasa and J. F.

Stoddart, *Org. Lett.*, 2009, **11**, 5238–41.
47 C. A. Murray, Z. Zhu, C. J. Cardin, H. M. Colquhoun and B. W. Greenland, *Supramol. Chem.* DOI: 10.1080/10610278.2017.1375113
48 L. Chen, H. Willcock, C. J. Wedge, F. Hartl, H. M. Colquhoun and B. W. Greenland, *Org. Biomol. Chem.*, 2016, **14**, 980–988.
49 L. Chen, F. Hartl, H. M. Colquhoun and B. W. Greenland, *Tetrahedron Lett.*, 2017, **58**, 1859–1862.
50 L. Chen, E. Vivier, C. J. Eling, T. S. Babra, J. G. Bouillard, A. M. Adawi, D. M. Benoit and H. M. Colquhoun, *Synth. Met.*, 2018, **241**, 31–38.
51 T. Zincke, G. Heuser and W. Möller, *Justus Liebigs Ann. Chem.*, 1904, **333**, 296–345.
52 N. Zeghbib, P. Thelliere, M. Rivard and T. Martens, *J. Org. Chem.*, 2016, **81**, 3256–3262.
53 T.-G. Zhan, T.-Y. Zhou, F. Lin, L. Zhang, C. Zhou, Q.-Y. Qi, Z.-T. Li and X. Zhao, *Org. Chem. Front.*, 2016, **3**, 1635–1645.
54 Y. Song, X. Huang, H. Hua and Q. Wang, *Dye Pigment*, 2017, **137**, 229–235.
55 O. Buyukcakir, S. H. Je, D. S. Choi, S. N. Talapaneni, Y. Seo, Y. Jung, K. Polychronopoulou and A. Coskun, *Chem. Commun.*, 2016, **52**, 934–937.
56 G. Das, T. Skorjanc, S. K. Sharma, F. Gándara, M. Lusi, D. S. Shankar Rao, S. Vimala, S. Krishna Prasad, J. Raya, D. S. Han, R. Jagannathan, J. C. Olsen and A. Trabolsi, *J. Am. Chem. Soc.*, 2017, **139**, 9558–9565.
57 Y. Fujioka, *Bull. Chem. Soc. Jpn.*, 1984, **57**, 3494–3506.
58 R. Welti, Y. Abel, V. Gramlich and F. Diederich, *Helv. Chim. Acta*, 2003, **86**, 548–562.
59 L. Liu, Y. Zhang and B. Xin, *J. Org. Chem.*, 2006, **71**, 3994–3997.
60 R. J. Rahaim and R. E. Maleczka, *Org. Lett.*, 2005, **7**, 5087–5090.
61 S. Basu, A. Coskun, D. C. Friedman, M. A. Olson, D. Benítez, E. Tkatchouk, G. Barin, J. Yang, A. C. Fahrenbach, W. A. Goddard and J. F. Stoddart, *Chem. Eur. J.*, 2011, **17**, 2107–2119.
62 F. M. Raymo, M. D. Bartberger, K. N. Houk and J. F. Stoddart, *J. Am. Chem. Soc.*, 2001, **123**, 9264–9267.
63 R. J. Mortimer, *Electrochim. Acta*, 1999, **44**, 2971–2981.
64 M. Krejčík, M. Daněk and F. Hartl, *J. Electroanal. Chem.*, 1991, **317**, 179–187.
65 E. M. Kosower and J. L. Cotter, *J. Am. Chem. Soc.*, 1964, **86**, 5524–5527.
66 Addition of **9** to $\mathbf{4}^{4+}$ resulted in minimal complexation induced ^{1}H NMR shifts
67 D. Brynn Hibbert and P. Thordarson, *Chem. Commun.*, 2016, **52**, 12792–12805.
68 A. Einstein, *Ann. d. Phys.*, 1905, **322**, 549–560.
69 R. Evans, G. Dal Poggetto, M. Nilsson and G. A. Morris, *Anal. Chem.*, 2018, **90**, 3987–3994.
70 R. Evans, Z. Deng, A. K. Rogerson, A. S. McLachlan, J. J. Richards, M. Nilsson and G. A. Morris, *Angew. Chem. Int. Ed.*, 2013, **52**, 3199–3202.
71 A. Macchioni, G. Ciancaleoni, C. Zuccaccia and D. Zuccaccia, *Chem. Soc. Rev.*, 2008, **37**, 479–489.
72 Y. Cohen, L. Avram and L. Frish, *Angew. Chem. Int. Ed.*, 2005, **44**, 520–554.
73 A. Jerschow and N. Müller, *J. Magn. Reson.*, 1997, **125**, 372–375.
74 I. Swan, M. Reid, P. W. A. Howe, M. A. Connell, M. Nilsson, M. A. Moore and G. A. Morris, *J. Magn. Reson.*, 2015, **252**, 120–129.
75 T. M. Barbosa, R. Rittner, C. F. Tormena, G. A. Morris and M. Nilsson, *RSC Adv.*, 2016, **6**, 95173–95176.
76 M. Nilsson, *J. Magn. Reson.*, 2009, **200**, 296–302.
77 AgilentTechnologies, *CrysAlis Pro User Manual*, 2013, vol. 44.
78 L. Palatinus and G. Chapuis, *J. Appl. Cryst.*, 2007, **40**, 786–790.
79 P. W. Betteridge, J. R. Carruthers, R. I. Cooper, K. Prout and D. J. Watkin, *J. Appl. Cryst.*, 2003, **36**, 1487.
80 P. Van Der Sluis and A. L. Spek, *Acta. Cryst.*, 1990, **A46**, 194–201.
81 M. J. Frisch, G. W. Trucks, H. B. Schlegel, *et. al.*, Gaussian 09, Revision D.01, Gaussian, Inc.: Wallingford CT, USA, 2009.
82 J. P. Perdew, K. Burke and M. Ernzerhof, *Phys. Rev. Lett.*, 1996, **77**, 3865–3868.
83 C. Adamo and V. Barone, *J. Chem. Phys.*, 1999, **110**, 6158–6170.
84 S. Grimme, S. Ehrlich and L. Goerigk, *J. Comput. Chem.*, 2011, **32**, 1456–1465.
85 R. Krishnan, J. S. Binkley, R. Seeger and J. A. Pople, *J. Chem. Phys.*, 1980, **72**, 650–654.
86 P. J. Hay, *J. Chem. Phys.*, 1977, **66**, 4377–4384.
87 M. Cossi, N. Rega, G. Scalmani and V. Barone, *J. Comput. Chem*, 2003, **24**, 669–681.